

# Theoretical and experimental investigation of an ammonia–water power and refrigeration thermodynamic cycle

G. Tamm<sup>a,\*</sup>, D.Y. Goswami<sup>a</sup>, S. Lu<sup>a</sup>, A.A. Hasan<sup>b</sup>

<sup>a</sup> Department of Mechanical Engineering, University of Florida, P.O. Box 116300, Gainesville, FL 32611-6300, USA

<sup>b</sup> Department of Mechanical Engineering, Birzeit University, P.O. Box 14, Birzeit, Palestinian Authority, Via Israel

Received 17 January 2003; accepted 25 August 2003

## Abstract

A combined thermal power and cooling cycle proposed by Goswami is under intensive investigation, both theoretically and experimentally. The proposed cycle combines the Rankine and absorption refrigeration cycles, using a binary ammonia–water mixture as the working fluid. This cycle can be used as a bottoming cycle using waste heat from a conventional power cycle or an independent cycle using low temperature sources such as geothermal and solar energy. Initial parametric studies of the cycle showed the potential for the cycle to be optimized for first or second law efficiency, as well as work or cooling output. For a solar heat source, optimization of the second law efficiency is most appropriate, since the spent heat source fluid is recycled through the solar collectors. The optimization results verified that the cycle could be optimized using the generalized reduced gradient method. Theoretical results were extended to include realistic irreversibilities in the cycle, in preparation for the experimental study. An experimental system was constructed to demonstrate the feasibility of the cycle and to compare the experimental results with the theoretical simulation. Results showed that the vapor generation and absorption condensation processes work experimentally. The potential for combined turbine work and refrigeration output was evidenced in operating the system. Analysis of losses showed where improvements could be made, in preparation for further testing over a broader range of operating parameters. © 2003 Elsevier Ltd. All rights reserved.

## 1. Introduction

Multi-component working fluids in power cycles exhibit variable boiling temperatures during the boiling process which make them suitable for a sensible heat source (Ibrahim and Klein, 1996; Kalina, 1984). The temperature difference between the heat source and the working fluid remains small to allow for a good thermal match between the source and working fluid, such that less irreversibility results during the heat addition process.

A novel ammonia–water binary mixture thermodynamic cycle capable of producing both power and

refrigeration has been proposed by Goswami (1998). An ammonia–water mixture is used as it exhibits desirable thermodynamic properties in terms of a large heat capacity. Ammonia is relatively inexpensive, can accommodate system design modifications well and separates easily from internal lubricating oils (Norton, 2001). Ammonia is also environmentally benign in comparison to other binary mixtures used in industry.

A schematic of the cycle is shown in Fig. 1. The relatively strong basic solution of ammonia–water leaves the absorber as saturated liquid at the cycle low pressure. It is pumped to the system high pressure and is preheated before entering the boiler by recovering heat from the weak solution returning to the absorber. As the boiler operates between the bubble and dew point temperatures of the mixture at the system high pressure, partial boiling produces a high concentration saturated

\* Corresponding author.

E-mail address: [solar@mae.ufl.edu](mailto:solar@mae.ufl.edu) (G. Tamm).

### Nomenclature

$E_c$	exergy of refrigeration
$m$	mass flow rate
$P$	pressure
$Q_c$	cooling capacity of the refrigeration unit
$Q_h$	total heat addition to the basic solution
$T$	temperature
$T_0$	ambient temperature

$T_c$	low temperature obtained after expansion
$W_{\text{net}}$	net work output from the turbine and pump
$x$	mass fraction of ammonia
$\Delta E_{\text{hs}}$	change in exergy of the heat source
$\eta_1$	first law efficiency
$\eta_2$	second law efficiency

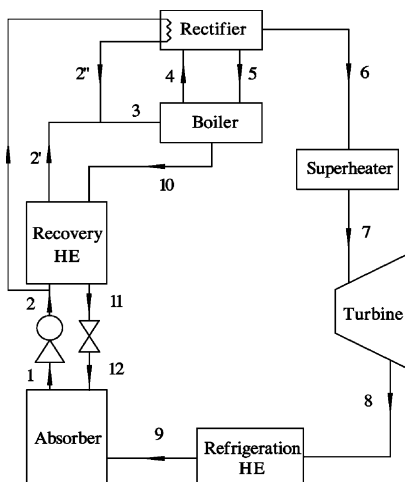


Fig. 1. Schematic of the power and cooling cycle, as used in the theoretical studies.

vapor and relatively low concentration saturated liquid. The liquid weak solution gives up heat in the recovery unit and throttles into the absorber. The rectifier condenses out water to further purify the vapor, by rejecting heat to a secondary strong solution stream, before entering the boiler. The vapor is superheated and expanded through the turbine to produce work. Due to the low boiling point of ammonia the vapor expands to low temperatures yielding the potential for refrigeration. The vapor is finally absorbed back into the liquid, giving off heat as the cycle heat output.

The main parameters that can be varied to influence the cycle are the heat source temperature, system high pressure, basic solution mass fraction, and absorber pressure and temperature. Saturation in the absorber reduces the number of independent main parameters to four that govern the cycle. Rectifier and superheater temperatures can also be modified, and the conditions of heat transfer from the source to the ammonia–water mixture as well.

The cycle can be driven by different heat sources including solar, geothermal, and low temperature waste

heat. The use of mid- and low-temperature solar collectors to drive the combined cycle was investigated by Goswami and Xu (1999), while using geothermal energy as a heat source was analyzed by Goswami et al. (2001).

Typical working conditions of a 400 K boiler temperature superheated to 410 K and an ambient at 280 K yields a first law efficiency of 23.5%. In comparison, the Carnot efficiency is 31.7% in operating between reservoirs at 410 and 280 K. Conventional power cycles if operating between the same temperatures would have lower first law efficiencies. At higher temperatures, their thermal efficiencies are better in comparison. However, the strength of this cycle lies in the improved heat source utilization. It exhibits much higher second law efficiencies than conventional power cycles.

## 2. Property evaluation

There are several studies on the evaluation of ammonia–water mixture properties in the literature. A convenient semi-empirical scheme is used here that combines the Gibbs free energy method for mixtures and bubble and dew point temperature correlations for phase equilibrium. The calculated results have been compared to experimental mixture properties in the literature with good agreement (Xu and Goswami, 1999).

## 3. Theoretical study

A parametric analysis is performed to assess individual parameter effects on the performance of the ideal cycle, and to verify that optimization is possible. Optimization of the cycle locates the operating conditions for the optimal ideal cycle performance. Inclusion of losses in an irreversibility analysis approaches the performance of a real cycle.

### 3.1. Parametric analysis

Operating conditions were individually varied in a straightforward parametric analysis to study the effects

on the energy transfers and efficiencies of the power and cooling cycle (Goswami and Xu, 1999). The parametric analysis gave insight into the behavior of the cycle, and showed that optimization of the cycle would be possible for first or second law efficiency, as well as work or cooling output. Fig. 2 is a sample of the parametric study, showing a peak in thermal efficiency within the range of operation.

The cycle first law or thermal efficiency is defined as the useful energy output divided by the total energy input, given by Eq. (1).

$$\eta_1 = \frac{W_{\text{net}} + Q_c}{Q_h} \quad (1)$$

The net work includes both the turbine output and pump input.  $Q_c$  is the refrigeration capacity and  $Q_h$  is the total heat added to the cycle from the heat source in both the boiler and superheater. These are calculated based on simple mass and energy balances over the cycle components.

Fig. 2 shows that for higher ammonia mass fractions in the basic solution, more vaporization occurs for the given boiler temperature and pressure. A higher vapor fraction allows for greater flow through the turbine, and more work production for a higher thermal efficiency. Fig. 3 concludes that more vapor is available for refrigeration output also, per kg of basic solution that is boiled.

For increasing turbine inlet or system high pressure, the figures show that the work and cooling outputs peak. Determining the location of these peaks is necessary a priori to optimize a working system's performance. Initially, increasing the system high pressure

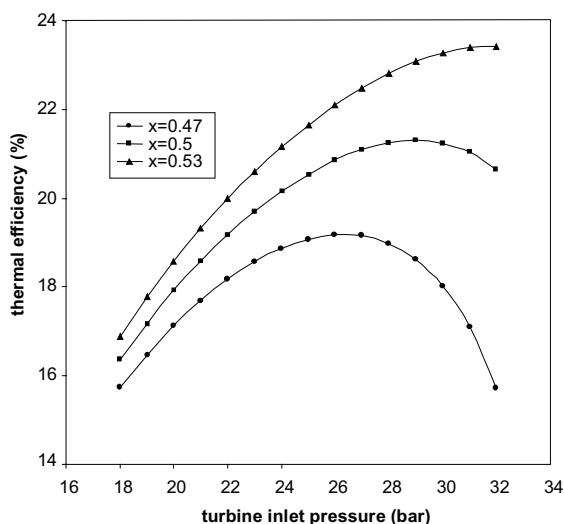


Fig. 2. Effect of turbine inlet pressure on the thermal efficiency (%) of the cycle.

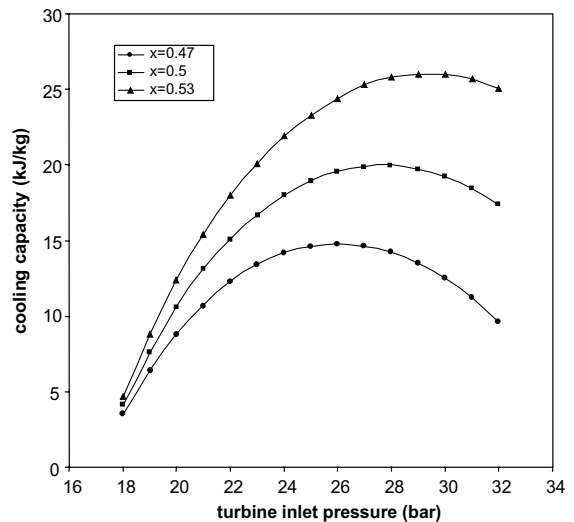


Fig. 3. Effect of turbine inlet pressure on the cooling capacity (kJ/kg) of the cycle.

while holding other parameters constant increases the pressure ratio across the turbine, such that there is more expansion work and lower turbine exit temperatures. However, the effect of the higher pressure limiting vapor production begins to dominate as the boiler exit fluid is shifted towards saturated liquid. The peak shifts for higher basic solution mass fractions as a two-phase equilibrium can be sustained at higher pressures for higher mass fractions.

Figs. 2 and 3 were evaluated for a boiler at 400 K, superheater at 410 K, absorber at 280 K and rectifier at 360 K. The low pressure in the system at the absorber was set at 2 bar. Note that a series of similar plots can be determined by changing any of the operating parameters. Each plot could conceivably provide a visual location of the optimum over the range of interest for the single parameter. For practical operation, the cycle has several parameters that are varied together, presenting a multi-dimensional surface on which an optimum can be found. A mathematical approach at locating this optimum is necessary, as the resulting surface cannot be visualized.

### 3.2. Optimization

For a solar heat source, optimization of the cycle for maximum second law efficiency is most appropriate as the heat source fluid is recycled back to the solar collectors at a temperature that is higher than the ambient. The unused exergy is not wasted.

Exergy, or availability, is defined as the maximum reversible work a substance can do during the process of reaching equilibrium with its environment. The second

law efficiency is defined as the exergy output divided by the exergy input to the cycle (Cengel and Boles, 1998). The exergy input is taken as the available energy change of the heat source. The exergy output is the exergy of the net work and the exergy of the refrigeration. The second law or exergy efficiency is given by Eq. (2).

$$\eta_2 = \frac{W_{\text{net}} + E_c}{\Delta E_{\text{hs}}} \quad (2)$$

The exergy of refrigeration,  $E_c$ , is the refrigeration capacity divided by the coefficient of performance of a Carnot refrigeration cycle operating between the ambient and cycle low temperatures, as given by Eq. (3) (Szargut et al., 1988).

$$E_c = Q_c \frac{(T_0 - T_c)}{T_c} \quad (3)$$

### 3.2.1. Optimization methodology

A generalized reduced gradient (GRG) scheme is used for the optimization, as discussed by Goswami et al. (2001). The GRG method searches a feasible region bounded by equality and inequality constraints. Moving finitely towards a better value with a newly determined search direction at every step, the optimum is ultimately reached within a limit of convergence.

The optimization scheme searches over eight free variables for the optimal second law efficiency as defined by Eq. (2). The parameters are the absorber or ambient temperature, boiler, superheater and rectifier temperature, the boiler pressure (high pressure), absorber pressure (low pressure), and heat source inlet and exit temperatures. From these eight free variables all other state points in the cycle can be determined with minimal and reasonable assumptions.

### 3.2.2. Optimization results

The desired heat source temperature will vary according to the intended use of the cycle. The effects of heat source temperature on the optimized cycle performance are shown in Figs. 4–7, optimized for second law efficiency. The refrigeration as a fraction of the heat addition,  $Q_c/Q_h$ , changes little as the heat source temperature increases as shown in Fig. 4. As the heat source temperature approaches the ambient temperature, refrigeration approaches zero. The highest refrigeration fraction is near a source temperature of 390 K. The refrigeration fraction decreases to zero near 480 K, as the higher temperature vapor can no longer be expanded to sub-ambient temperatures.

The net power as a fraction of heat addition,  $W_{\text{net}}/Q_h$ , increases as the heat source temperature increases. As the turbine work output is related mainly to the pressure ratio across the turbine, the net power curve can be explained in relation to pressure ratio in Fig. 5, which

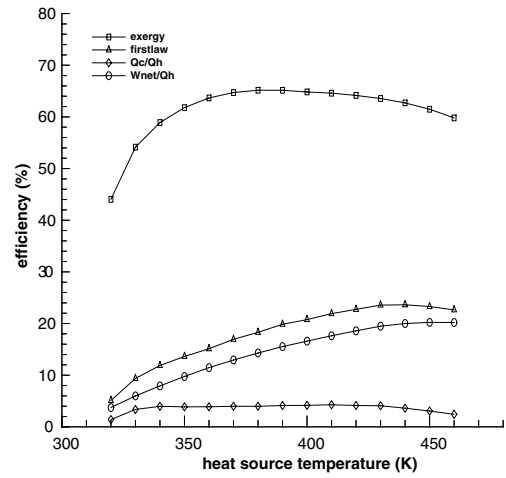


Fig. 4. Efficiencies of the optimized cycle at various heat source temperatures, optimized for second law efficiency.

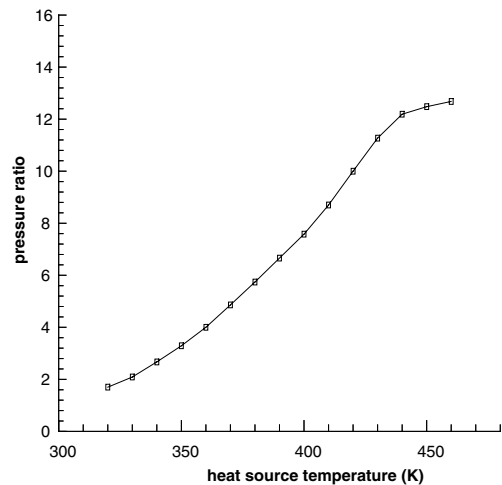


Fig. 5. Pressure ratio of the optimized cycle at various heat source temperatures, optimized for second law efficiency.

shows a continuous increase with heat source temperature.

The first law efficiency curve, which is a sum of the refrigeration and power curves, shows similar behavior to the power curve up to the maximum value of 23.6% at 400 K. After the maximum point, the efficiency starts decreasing slowly in a similar manner to the refrigeration curve.

The second law or exergy efficiency shows a maximum value of 65.2% at 380 K. The sharp increase in Fig. 4 of the second law efficiency between 320 and 380 K is due to the increase of both power and refrigeration outputs. The second law efficiency reaches a maximum

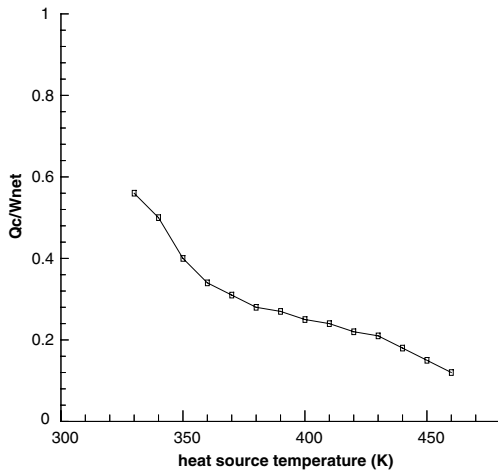


Fig. 6. Ratio of refrigeration to work of the optimized cycle at various heat source temperatures, optimized for second law efficiency.

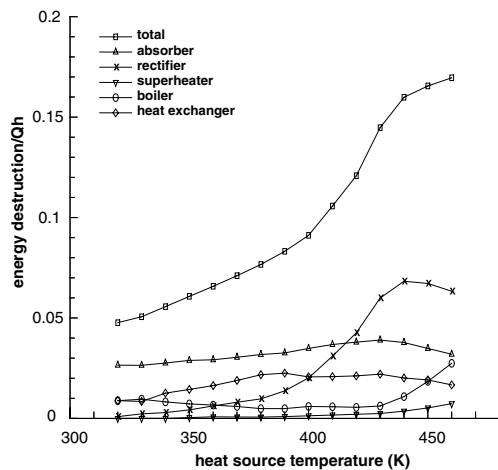


Fig. 7. Exergy destruction of the optimized cycle at various heat source temperatures, optimized for second law efficiency.

where the refrigeration output begins to decrease above 400 K.

Fig. 6 shows the refrigeration to net power ratio versus the heat source temperature. In the temperature range between 320 and 360 K this ratio changes rapidly, while above 360 K the ratio decreases slowly, reaching 0.12 at 460 K. Thus, increasing the heat source temperature favors the production of power rather than refrigeration.

Fig. 7 shows the normalized exergy destruction in the cycle as a function of the heat source temperature. The total exergy destruction in the cycle increases with an increase in the heat source temperature. It can be seen in

Fig. 7 that the exergy destruction in both the absorber and heat exchanger changes little as the source temperature increases. The superheater has almost no exergy destruction because of its small heat load. The boiler exergy destruction is much lower than that of the absorber. Exergy destruction in the rectifier increases throughout, as the heating load also increases in the rectifier. From the exergy analysis, if the heat source is between 320 and 460 K, then the best operating heat source temperature is around 380 K, since it gives the maximum exergy efficiency.

It has been shown that the cycle can be optimized for a range of heat source temperatures. Similarly, the cycle can be optimized for each heat sink or ambient temperature, and other parameters. Therefore, the cycle can be customized to the intended application for optimal performance.

### 3.3. Irreversibility analysis

In realistic systems, there are irreversibilities associated with every component as with this ammonia–water cycle. These irreversibilities will have negative effects on the performance of the cycle. The effects of each loss were studied individually and jointly on the cycle performance. Typical working conditions used in this analysis were 400 K and 30 bar at the boiler exit, 360 K rectification, 410 K at the turbine inlet, 280 K and 2 bar in the absorber, and a basic solution mass fraction of 0.53.

A typical turbine efficiency of 90% was assumed as suggested in the literature (Drbal et al., 1996). The thermal efficiency drops from 23.3% to 19.7%, a decrease of 15.4%. Due to the irreversibility in the turbine, although the pressure ratio is the same, the exhaust temperature of the turbine is higher. Less energy is converted into mechanical work in the turbine, and the turbine work output drops from 76.1 to 68.5 kW, a decrease of 10.0%. At the same time, a higher turbine exhaust temperature provides less cooling capacity. The cooling capacity drops 29.2% from 26.0 to 18.4 kW.

An 80% pump efficiency was assumed as suggested in the literature (Drbal et al., 1996). The pump work requirement increases from 3.4 to 4.2 kW. This small increase causes the thermal efficiency to drop slightly.

A pressure loss of 5% of the inlet pressure was assumed across the boiler as suggested in the literature (Bhatt et al., 1994). The results show this pressure loss has almost no negative effect on the cycle performance. Only slightly more pump work is required to boost the boiler inlet pressure to compensate for the pressure loss in the boiler.

A pressure loss of 5% was assumed for the superheater (Bhatt et al., 1994). The results show only a minor negative effect on the cycle performance. Thermal efficiency decreases by 3% of that in the ideal cycle, from

23.3% to 22.6%. Due to the pressure loss in the superheater, the turbine inlet pressure drops. Therefore, less expansion is possible producing 1.2% less work and higher exhaust temperatures. The cooling capacity decreases by 6.5%.

A pressure loss of 5% was assumed for both streams in the recovery heat exchanger (Bhatt et al., 1994). The effects on the cycle performance are minimal, with a negligible decrease in thermal efficiency owing to an increase in the pump work requirement.

A pressure loss of 5% was assumed in the refrigeration heat exchanger, for comparison to other component pressure losses. The thermal efficiency drops by 2.6% from 23.3% to 22.7%, as the higher turbine exhaust pressure limits the expansion possible. The work output decreases by 1.6%. The reduced turbine pressure ratio also raises the exhaust temperature, reducing the cooling capacity by 4.6%. In a typical cooler, however, the heat exchanger experiences a 3% pressure loss (Bhatt et al., 1994), which is the value used in the combined irreversibility study.

Finally, the overall effect of the irreversibility associated with the cycle was analyzed for combined losses. The thermal efficiency decreases by 20.6%, from 23.3% under ideal conditions to 18.5%. The turbine work output drops by 11.8%, from 76.1 to 67.1 kW. The cooling capacity decreases by 37.7%, from 26.0 to 16.2 kW. It can be seen that the greatest loss is attributed to the expansion in the turbine not being isentropic.

#### 4. Experimental study

The theoretical study was necessary to investigate the potential for the combined power and cooling cycle concept. An experimental study is necessary to demonstrate the combined power and cooling cycle and to compare the experimental results with the theoretical simulation. Demonstration of the vapor generation, expansion and absorption processes verifies the cycle concept and provides greater insight into the fundamentals of binary fluid systems. Operation of a working system gives practical experience and a means to improve the basic cycle design, furthering the concept towards industry.

##### 4.1. Experimental setup

An experimental system has been built to demonstrate the cycle, according to the schematic shown in Fig. 8. The rectifier has been left out from the original cycle concept in Fig. 1 for simplicity, as purification of the high concentration ammonia–water vapor is not critical in these initial tests. As there is no rectification, neither is there a need for superheating the vapor entering the turbine. The strong solution of ammonia–

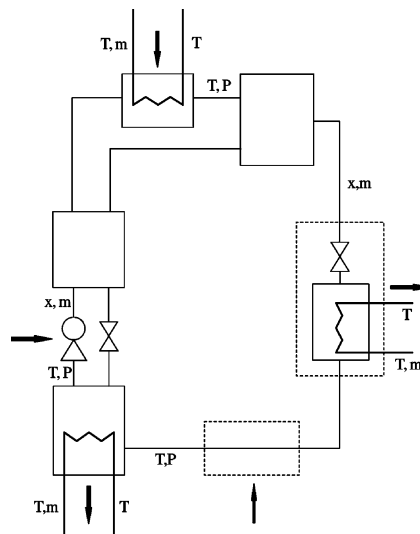


Fig. 8. Schematic of the power and cooling cycle, as used in the experimental studies.

water is pumped from the absorber with a rotary vane positive displacement pump capable of producing the high boiler pressures of interest. Leaving the pump, the strong solution passes through a vertical stacked plate heat exchanger where it recovers heat from the weak solution returning to the absorber. The boiler is also a vertical stacked plate heat exchanger, using resistance heated hot water to partially boil the strong solution which flows into a simple carbon steel tank where gravity separates out the liquid from the vapor. The boiler is capable of producing water temperatures replicable by solar, geothermal and low-temperature waste heat sources.

The relatively low concentration weak solution exits the bottom of the separator while the high concentration vapor leaves through the top. The weak solution flows through the solution heat exchanger to yield energy to the strong solution. After a throttling valve to reduce pressure, the weak solution enters at the top of the absorber through a spray nozzle across the cooling elements inside. The cooling is provided by a 50% ethylene–glycol and water mixture, capable of simulating heat rejection to the ambient. This simulation of the ambient is for convenience and reliability. The cooling elements are finned car evaporators through which coolant flows, placed in parallel above the liquid pool. The ammonia vapor that is not absorbed as it bubbles into the liquid pool is absorbed above the pool into the liquid weak solution passing over the cooling elements.

A heat exchanger and throttling valve simulate the expansion process of the turbine, until a turbine is procured for later testing and investigation of the expansion process. The vapor is throttled and passes

through a stacked plate heat exchanger against coolant flow. The refrigeration unit is also represented by the turbine heat exchanger. This simulated turbine lowers the pressure and temperature of the vapor before it enters the carbon steel absorber through a series of small holes, intended to bubble the vapor into the absorber liquid pool for better absorption.

Stainless steel tubing and fittings connect the components. Care was taken to minimize flow losses in the system. All the tubing is insulated, as are the absorber and separator tanks. Preventing heat losses in vapor lines discourages condensation on the tubing walls.

Pressures, temperatures, mass fractions and mass flow rates are recorded at locations shown in Fig. 8. Properties at all other state points can be extrapolated with minimal assumptions. However, redundant measurements are taken from other locations to compare energy transfers calculated from property data on the working fluid side of components with those calculated from the heat source and coolant sides. The energy transfers will not be in agreement if there is error in the data measurement or property correlation, if a fluid is not in its expected phase, or if equilibrium is not achieved in the system.

Real-time and time-averaged data are recorded from pressure transducers and T-type thermocouples by the data acquisition system. Samples are taken by syringe through septum ports in the vapor, weak and strong solution lines, and analyzed by a gas chromatograph in the lab using a thermal conductivity detector. Flow meters are in place to measure vapor, weak and strong solution, heat source and coolant flow rates. The liquid levels in the absorber and separator are monitored through site glasses.

#### 4.2. System simulation

The main parameters that can be varied to influence the cycle are the boiler temperature, system high pressure, basic solution mass fraction, and absorber pressure and temperature. Saturation in the absorber reduces the number of independent main parameters to four that govern the cycle. In the experimental study, the effect of the heat source on the working fluid was of greater interest than how the heat source interacted with the system. Therefore the source conditions were not controlled as rigorously as the working fluid conditions entering and exiting the boiler.

A computer program has been written allowing calculation of thermodynamic properties, cycle design and data analysis. The program evolves with the experiment, incorporating observed irreversibilities to expedite designing each experiment prior to running it and to minimize time to steady state. The program handles data analysis efficiently, and provides clear comparison to expected results.

The range of operating parameters is dictated by experimental and practical limits. The heat source can be varied up to 110 °C in this system, which is typical for solar or geothermal applications, based on a pump temperature limit. For the low heat source temperature limit, vaporization is possible only at low pressures. The work output suffers however, and investigation of very low heat source temperatures is not of major interest. The lower limit is arbitrarily set at 40 °C, below which the heat source loses its effectiveness greatly. The absorber rejects heat to the ambient in principal, and so the absorber temperature cannot be arbitrarily low. Internal constraints are that the system high pressure is limited to 200 psig (14.8 bar), corresponding to the separator pressure rating, and the absorber pressure to 30 psig (3.1 bar) according to its pressure rating. The lower limit of the boiler pressure is arbitrary, provided it is above the saturation pressure in the absorber. The basic solution mass fraction may vary between 0 and 1, provided the mixture can be partially evaporated at the given boiler pressure and temperature.

Limits of vapor generation for a typical solution concentration are shown in Fig. 9, which gives the vapor fraction of the mixture leaving the boiler for various temperatures and pressures. The boiler temperature must be high enough to partially boil the strong solution at the given pressure and mass fraction, to generate vapor for power and refrigeration production. However

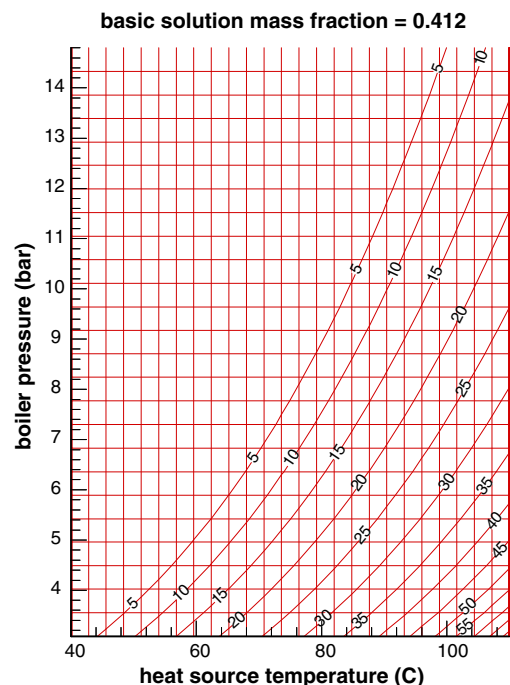


Fig. 9. Vapor fraction (%) of the ammonia–water fluid leaving the boiler, based on simulation.

if too high, there will be no liquid leaving the separator and the cycle will resemble a binary fluid Rankine cycle.

Figures similar to Fig. 9 aid in designing a desired set of experiments, by knowing a priori whether the desired operating conditions are within the range of practical limits of heat addition, heat rejection, work and refrigeration output. Fig. 10 can be used as a guideline to obtain refrigeration output. As in Fig. 9, refrigeration

output is possible only if vapor is produced in the boiler. However for high boiler temperatures, the expansion cannot lower the high vapor temperature to sub-ambient conditions, and no refrigeration output is witnessed. There is less refrigeration output if the ambient temperature is higher, which raises the absorber saturation pressure for a given basic solution mass fraction and thus decreases the pressure ratio across the turbine.

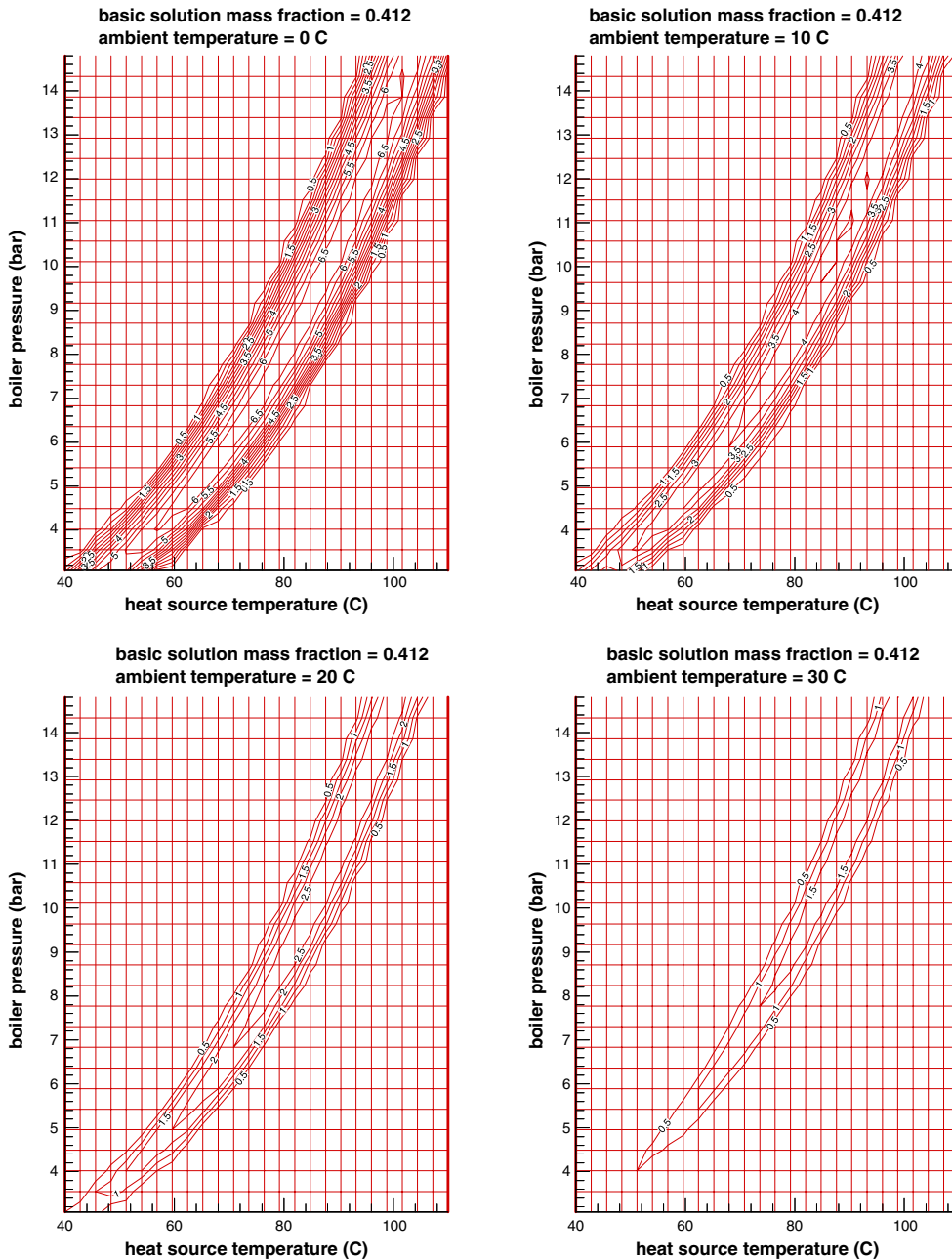


Fig. 10. Refrigeration output (kJ/kg) per unit basic solution flow, based on simulation.

### 4.3. Experimental results

Experimental results show the system to work. Vapor generation at high pressures verifies that the system can produce work from heat. Modeling the turbine and refrigeration unit, experiments support that refrigeration can be produced for certain operating parameters. Absorption of the vapor into the weak solution verifies the basic solution can regenerate itself.

The boiler pressures and temperatures were varied over a range sufficiently large to show trends in system performance and to compare them to simulations. A basic solution mass fraction of 41.2% was selected for simplicity. For simulating the ambient temperatures of interest, a 40–50% mass fraction gives a range of absorber pressures most compatible with the current experimental system. The absorber temperature affects the absorber pressure, and thus the turbine expansion and refrigeration processes. The boiling process is not expected to depend highly on the absorber temperature and so only two absorber temperatures were studied.

In comparison to simulated results, experiments suggest that there are losses in the system and non-equilibrium phase change processes. Many of the results can be attributed to the wall temperatures in the boiler and solution heat exchanger being higher than the bulk temperature of the fluid being heated. This causes vapor production of lower mass fraction as higher temperature boiling can vaporize more water vapor, which has a higher boiling point than ammonia. After removal from the heat source, there is condensation in the relatively cooler bulk fluid and on vessel walls. This absorption serves to lower the vapor fraction of the fluid, and raise the bulk temperature. Again due to the boiling point of water, more water will condense than ammonia such that the remaining vapor will be of higher mass fraction and the liquid part will be of lower mass fraction. If it is simulated that the fluid exists in equilibrium leaving the heater at the bulk temperature, pressure and overall basic solution mass fraction, then the real fluid will have a lower enthalpy at the same bulk temperature, pressure and basic solution mass fraction since there is less vapor in the real fluid. Less boiling has occurred than expected. This effect is more prominent as the heater exit temperature is measured further downstream from the heater exit.

The system is at a higher temperature than the ambient at all points, as there is no expansion by a turbine and the fluid is never cooled to below the ambient temperature by a heat exchanger. Therefore, there will always be losses of heat to the surroundings. It is concluded that the most accurate assessment of the fluid properties is made where the fluid is subcooled liquid, as the phase is certain.

The total heating of the strong solution is by heat recovery from the weak solution and heat addition

from the hot water heat source. The weak solution and hot water remain liquid throughout, and the respective energy transfers as measured from their property changes are taken as accurate. Fig. 11 shows the total heating of the strong solution from the absorber temperature of 15 °C to the conditions leaving the boiler. The simulated plot assumes that the strong solution exits the boiler at equilibrium. As expected, there is less total heating for higher boiler pressures as there is less vaporization possible. For higher temperatures, there is more total heating as the fluid can hold more vapor. The experimental results show that there is more condensation back into the bulk after the boiler in the higher temperature cases. Since the vapor mass fraction is lower for the higher boiler temperature, there will be more water bubbles which cannot sustain themselves in the relatively lower bulk temperature fluid.

It is interesting to note that the heat source temperature for all the cases was approximately the same, about 85–95 °C. If the heater wall produces roughly the same amount and ammonia mass fraction vapor, less of that vapor condenses for lower boiler temperatures as the bulk needs to be heated less and so the remaining vapor just cools but remains vapor. Hence for lower boiler temperature cases, the experimental fluid at the heater exit is closer to what is expected, and so is the total heat input.

The theoretical study assumes a maximum heat transfer from the weak solution to preheat the strong solution, with the weak solution exiting the recovery heat exchanger at the strong solution inlet temperature. In practice, an average temperature difference of 16 °C was found, leading to an average 53.6% recovery of possible heat from the weak solution.

The separator in the modeled cycle has no losses associated with it. However in the experiment the separator exhibits on average 9.2 kJ/kg exergy loss. Hence the separation is not into pure saturated liquid and pure saturated vapor as expected, but rather into high quality vapor and low quality liquid mixtures. The insulation of the separator walls has reduced the exergy loss by 30% from before insulation was added, but more insulation will be considered.

The reduction in vapor flow rate is mainly due to condensation in the bulk fluid and on the cooler separator walls. The vapor fraction is shown in Fig. 12. On average, 88% of vapor flow is realized, with the most reduction in higher boiler temperature cases. This reduction carries over to the work output and refrigeration, hurting the cycle.

As the boiler temperature increases, water vapor can more readily be formed so the vapor mass fraction decreases. As the vapor mass fraction is very high, the liquid loses more ammonia than water at higher boiling temperatures and the weak solution mass fraction

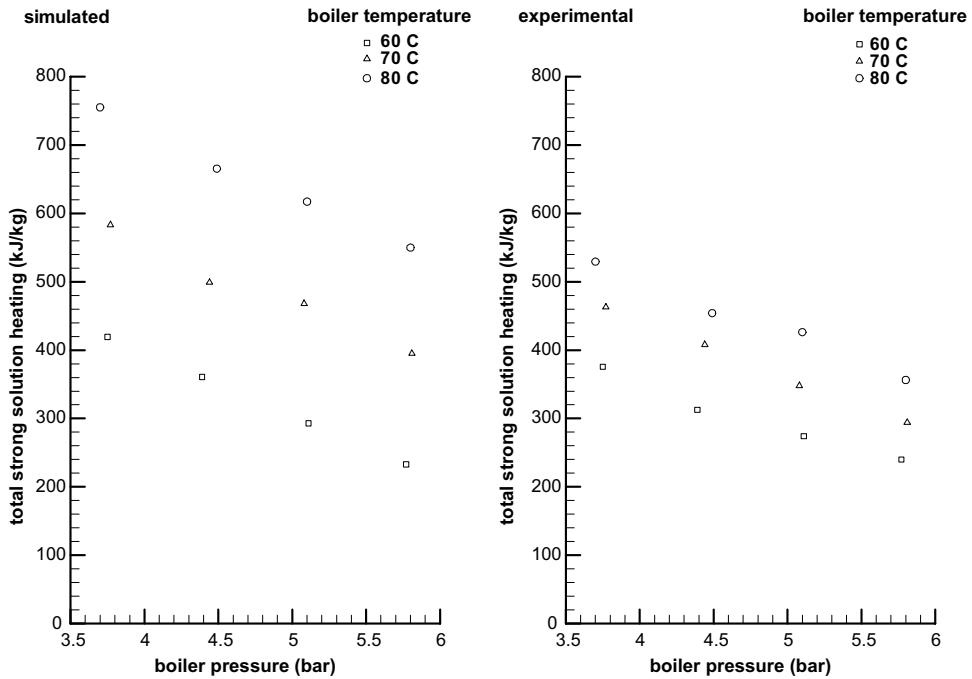


Fig. 11. Total heat input for various boiler temperatures and pressures. The absorber is at 15 °C.

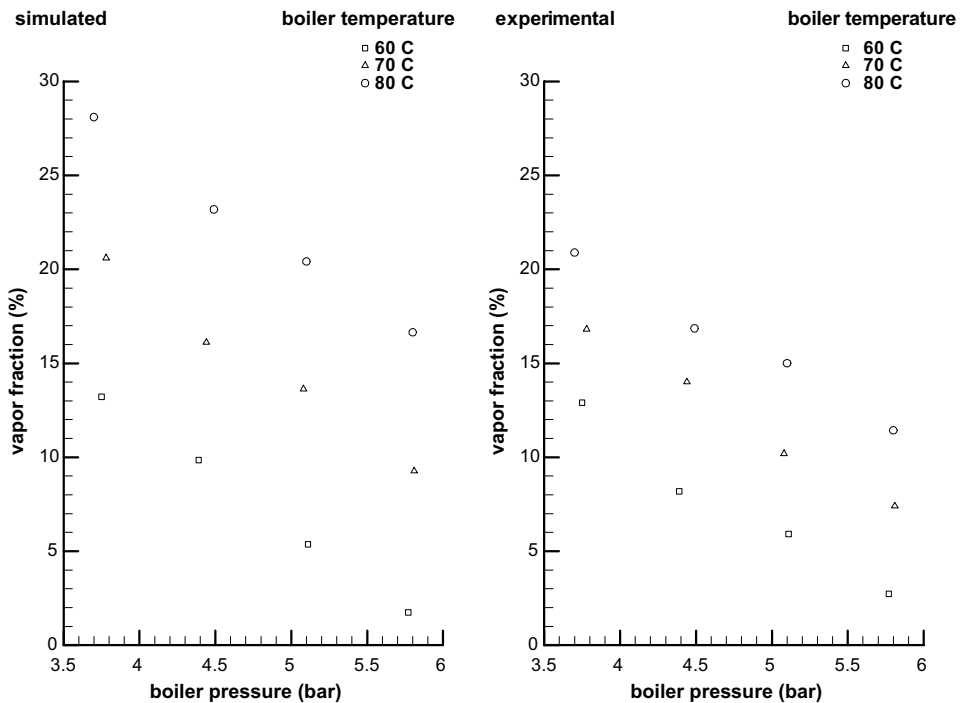


Fig. 12. Vapor fraction for various boiler temperatures and pressures. The absorber is at 15 °C.

decreases as well. The vapor mass fraction is shown in Fig. 13 and the weak solution mass fraction in Fig. 14.

The experimental vapor mass fractions are found to be higher than predicted, as water has condensed into the

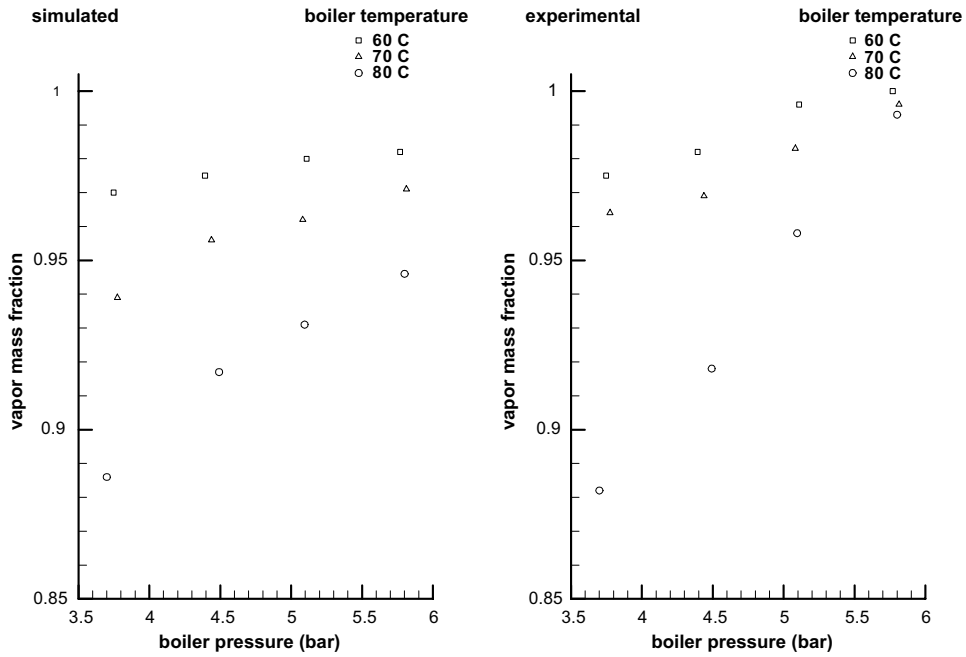


Fig. 13. Vapour mass fraction for various boiler temperatures and pressures. The absorber is at 15 °C.

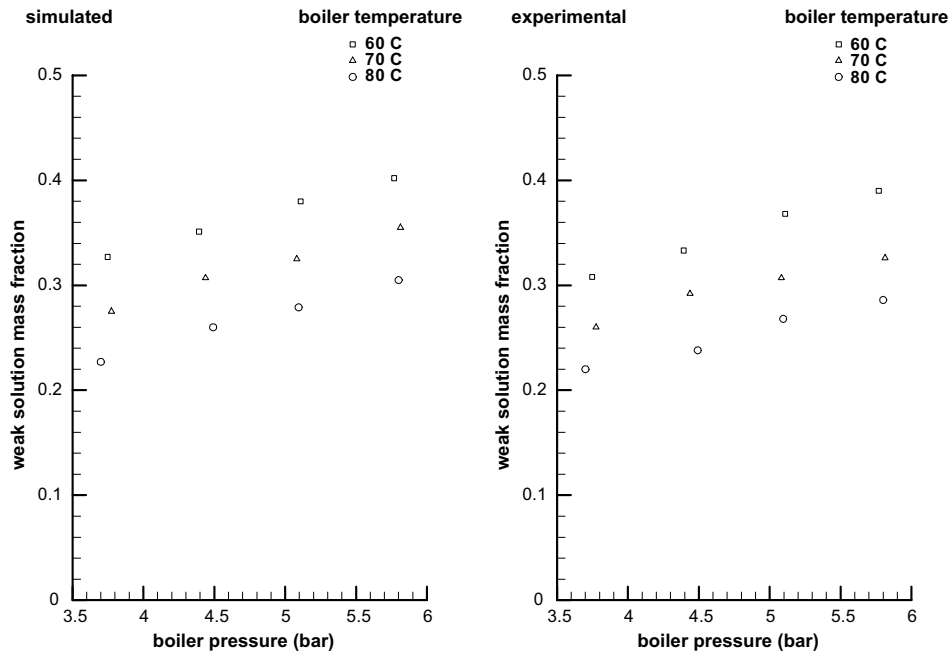


Fig. 14. Weak solution mass fraction for various boiler temperatures and pressures. The absorber is at 15 °C.

bulk and on cool surfaces more readily than the ammonia. The weak solution mass fractions are hence below what are expected.

It can be concluded that conditions leaving the separator in the vapor stream entertain the possibility of work and refrigeration production when the turbine and

refrigeration units are installed. Improvements to the system design to reduce losses, and improvements to the modeling of the boiling process will prepare the system for the next phase to testing.

## 5. Conclusions

Parametric analysis of the cycle showed the potential for the cycle to be optimized. Optimization of the operating parameters in the cycle is possible for each heat source and heat sink temperature, using a GRG method. The cycle may be optimized for the first law efficiency, second law efficiency, power output or cooling output, depending on the intended application and the heat source. For a solar heat source, optimization for the second law efficiency is most appropriate, since the spent heat source fluid is recycled back to the solar collectors. It was found from simulation that optimization of the cycle for second law efficiency produces no refrigeration at high heat source temperatures, while for low heat source temperatures it does. Inclusion of realistic losses in the analysis of the cycle reduces the cycle thermal efficiency by 20.6%, with 11.8% less work output and 37.7% less cooling capacity. The most significant source of irreversibility in the cycle is a non-isentropic expansion process in the turbine. An experimental system was constructed and successfully operated to demonstrate the feasibility of the combined power and cooling thermodynamic cycle. The results from test data compared well to simulations. Vapor generation and absorption condensation processes were shown to work experimentally. The potential for combined work and refrigeration output was evidenced. Addition of a turbine/generator set and a chiller/heat exchanger are needed to confirm this conclusion. An analysis of losses has shown where improvements can be made, for further testing over a broader range of operating parameters.

## Acknowledgements

The authors acknowledge funding from the US Department of Energy for work conducted at the University of Florida.

## References

- Bhatt, M.S., Srinivasan, K., Krishna, M.V., Seetharamu, S., 1994. Absorption–resorption heating cycles with the new working pairs R21-NMP and R21-DMA. *Energy Conversion Management* 35, 443–451.
- Cengel, Y.A., Boles, M.A., 1998. *Thermodynamics: An Engineering Approach*, third ed. McGraw-Hill Inc., New York.
- Drbal, L.F., Boston, P.G., Westra, K.L., Erickson, R.B., 1996. *Power Plant Engineering*. Chapman & Hall, New York.
- Goswami, D.Y., 1998. Solar thermal technology: present status and ideas for the future. *Energy Sources* 20, 137–145.
- Goswami, D.Y., Xu, F., 1999. Analysis of a new thermodynamic cycle for combined power and cooling using low and medium temperature solar collector. *ASME Journal of Solar Energy Engineering* 121, 91–97.
- Goswami, D.Y., Hasan, A.A., Lu, S., Tamm, G., 2001. Ammonia-based combined power/cooling cycle, UFME/SEEL Report 2001-05, University of Florida, Gainesville, FL.
- Ibrahim, O.M., Klein, S., 1996. Absorption power cycles. *Energy* 21, 21–27.
- Kalina, A.I., 1984. Combined cycle system with novel bottoming cycle. *Journal of Engineering for Gas Turbines and Power* 106, 737–742.
- Norton, E., 2001. Ammonia Liquid Recirculation. *ASHRAE Journal* 43 (10), 50–51.
- Szargut, J., Morris, D.R., Steward, F.R., 1988. *Exergy Analysis of Thermal, Chemical, and Metallurgical Processes*. Hemisphere Publishing Co., New York.
- Xu, F., Goswami, D.Y., 1999. Thermodynamic Properties of Ammonia Water Mixtures for Use in Power Cycles. *Energy (Oxford)* 24, 525–536.